Article

Hover Performance Analyses of Coaxial Co-Rotating Rotors for eVTOL Aircraft

Yu-Been Lee and Jae-Sang Park *

Department of Aerospace Engineering, Chungnam National University, 99 Daehak-ro, Yuseong-gu, Daejeon 34134, Korea; lyb0718@o.cnu.ac.kr
* Correspondence: aerotor@cnu.ac.kr; Tel.: +82-42-821-6682; Fax: +82-42-825-9225

Abstract: Hover performance analyses of coaxial co-rotating rotors (or stacked rotors), which can be used as lifting rotors for electric VTOL (eVTOL) aircraft, are conducted here. In this study, the rotorcraft comprehensive analysis code, CAMRAD II, is used with the general free-wake model. The generic coaxial co-rotating rotor without the blade taper and built-in twist is considered as the baseline rotor model, and the rotor is trimmed to match a prescribed rotor thrust value. The hover performance, including the rotor power and Figure of Merit (FM), is investigated for various index angles, axial spacings, blade taper ratios, and built-in twist angles. A maximum FM value is obtained near an index angle of $0°$ and $10°$ when the axial spacing is below and above 5.27%R, respectively. When the index angle is $0°$ and axial spacing is 1.44% R, the maximum increments in the FM are 3.03% and 6.06%, respectively, for a rotor with a blade taper ratio of 0.8 and a built-in twist angle of $-12°$. Therefore, this simulation study demonstrates that the hover performance of coaxial co-rotating rotors can be changed by adjusting the index angle or the axial spacing.

Keywords: eVTOL; coaxial co-rotating rotor; rotorcraft comprehensive analysis; free-wake model; hover performance analysis

1. Introduction

There are several problems associated with traffic congestion and environmental pollution in modern urban areas owing to high population densities. Urban Air Mobility (UAM) is considered a potentially viable transportation solution. Aircraft that are utilized for UAM require a vertical take-off–landing (VTOL) capability and outstanding aerodynamic performance [1]. In addition, structural safety and low acoustic noise are important issues for these aircraft because they are operated at relatively low altitudes in urban areas. Therefore, electric VTOL (eVTOL, Figure 1 [2]) aircraft have attracted significant attention for this application because of their advantages over conventional rotorcrafts, such as the simplicity of the drivetrain system, low acoustic noise, and safe operation in modern urban environments [3]. An eVTOL aircraft uses distributed electric propulsion (DEP) with a multi-rotor system.

The multi-rotor system can secure the safety of eVTOL aircraft because if one rotor fails in flight, there are backup rotors. Furthermore, because the rotor disk area is small, the multi-rotor system has a low noise signature [4]. The multi-rotor system for eVTOL aircraft usually uses coaxial rotors [5]. There are two types of coaxial rotors: One is the coaxial counter-rotating rotor, in which the upper and lower rotors rotate in opposite directions about the common axis of rotation; the other is the coaxial co-rotating rotor (or stacked rotor, Figure 2), in which the upper and lower rotors rotate in the same direction. Compared with the coaxial counter-rotating rotor, studies on the coaxial co-rotating rotor, which may be used as lifting rotors for eVTOL aircraft in hover and vertical flights [6], have been limited. The coaxial co-rotating rotor has two key design parameters, namely the index angle ($\Delta\Psi$) and the axial spacing (ΔZ), as shown in Figure 3. The index angle is the azimuthal spacing

between the upper and lower rotor blades, and the axial spacing is the distance between the upper and lower rotors along the axis of rotation. The index angle of the coaxial co-rotating rotor can be controlled and adjusted by each motor and clutch of the upper and lower rotors [1].
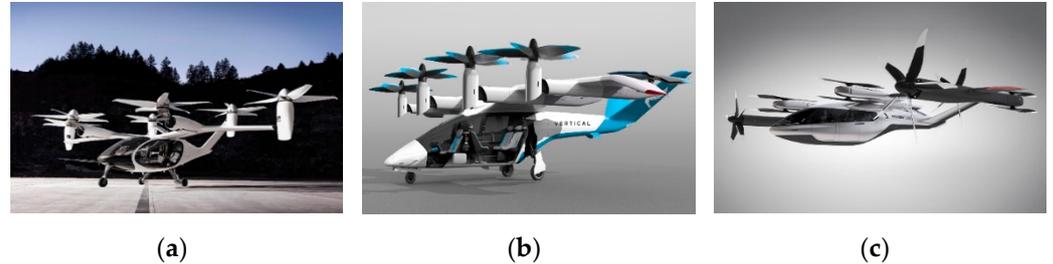

(**a**)   (**b**)   (**c**)

Figure 1. Various eVTOL aircraft with the multi-rotor system [2]: (**a**) Joby S4 (Joby Aviation); (**b**) VA-X4 (Vertical Aerospace); (**c**) S-A1 (Hyundai Motors).

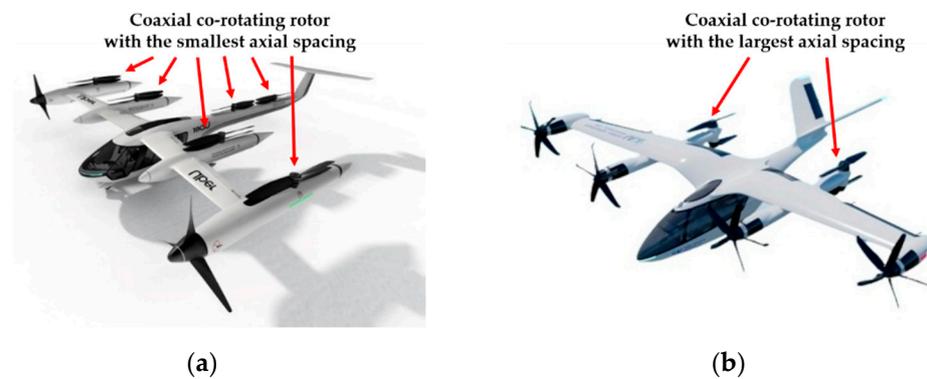
(**a**)   (**b**)

Figure 2. Coaxial co-rotating rotors with different axial spacings for eVTOL aircraft: (**a**) Uber; (**b**) Korea Aerospace Industries.
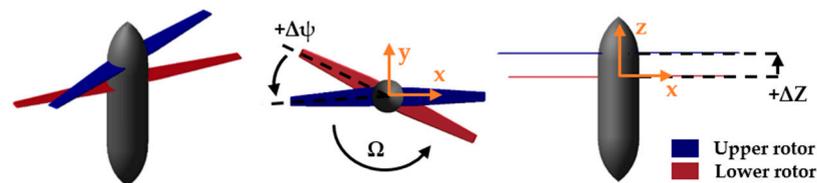

Figure 3. Index angle ($\Delta\Psi$) and axial spacing (ΔZ) for coaxial co-rotating rotor.

The coaxial co-rotating rotor can improve the hover performance efficiency and reduce acoustic noise during operation using the two key design parameters [1,7,8]. Furthermore, the slipstream boundary or blade tip vortex for the coaxial co-rotating rotor can be altered for the index angle [9,10]. The AH-64A Apache helicopter's tail rotor uses a coaxial co-rotating rotor with an index angle of 55° to reduce the acoustic noise for comparison with conventional rotor configurations [11]. The previous analysis [12] showed that the sound pressure level of the coaxial co-rotating rotor decreased by 5 dB when the index angle increased from 0° to 90°. In addition, it was concluded that the thickness noise could decrease at a specific index angle region [13]. Considering the advantages of the coaxial co-rotating rotor, simulation and experimental studies on the hover performance were conducted [1,14–21].

Previous studies [14–21] were conducted on the hover performance of a coaxial co-rotating rotor, with the index angles and axial spacings based on the Rotorcraft Comprehensive Analysis System (RCAS [22]), computational fluid dynamics (CFD), and experimental measurements. Unlike the coaxial counter-rotating rotor that satisfies the balance of the entire rotor torque, the coaxial co-rotating rotor does not achieve a torque balance because

the upper and lower rotors rotate in the same direction. Hence, most studies on the performance analyses in hover used the trim approach to satisfy the torque of the upper or lower rotor of a coaxial counter-rotating rotor [14–19]. In these studies, it was discovered that there existed an optimal index angle for a coaxial co-rotating rotor, which resulted in a better hover performance compared with that of the coaxial counter-rotating rotor for both experimental and numerical results [14]. Based on both the experimental and computational studies, it was established that the hover performance of a coaxial co-rotating rotor significantly depended on the index angle [15]. A previous paper [16] found that an important factor in the performance improvements for a coaxial co-rotating rotor was the induced inflow. Furthermore, previous research [17] determined that the induced power of a coaxial co-rotating rotor was approximately 4% lower than that of a coaxial counter-rotating rotor at an index angle of $10°$. Former studies [18,19] observed the relationship between the axial spacing and hover performance of coaxial co-rotating rotors. A previous work [18] showed that the thrust sharing between the upper and lower rotors could be varied by adjusting the axial spacing. The aerodynamic interference between the upper and lower rotors was experimentally studied by comparing the coaxial counter-rotating rotor, coaxial co-rotating rotor, and single rotor [18]. Experimental results showed that the performance losses for the coaxial co-rotating rotor decreased with the axial spacings [19].

The trim of the coaxial co-rotating rotor was not considered in the hover performance analyses using RCAS with the viscous vortex particle method (VVPM), CFD, and experimental studies [20,21]. When the collective pitch angle of both the upper and lower rotors was fixed, it was found that the hover efficiency for a large axial spacing was approximately 10% higher compared with the case of a small axial spacing [20]. Moreover, it was shown that the hover efficiency improved by approximately 2% to 4% close to an index angle of $0°$ [20]. Further investigations were conducted in [21] based on [20]. In previous studies on hover performance analyses [14–21], the coaxial co-rotating rotor was trimmed to satisfy a given torque value, or a trim approach was not used with the constant collective pitch angle. However, to the best of our knowledge, there have been no published papers that consider the trim of the coaxial co-rotating rotor to match the prescribed rotor thrust value, although the rotor thrust is the most fundamental and important target for the rotorcraft trim. Furthermore, there have been no previous studies on the hover performance of coaxial co-rotating rotors using the rotorcraft comprehensive analysis code, CAMRAD II [23], with the free-wake model. Although the unsteady lifting-line theory along with the free-wake model in CAMRAD II is a lower-order aerodynamics model compared to the RCAS with VVPM and CFD, it may provide reasonable prediction results for the hover performance of a coaxial co-rotating rotor. The authors of this paper conducted hover performance analyses for a coaxial co-rotating rotor based on the Harrington rotor, using CAMRAD II with the free-wake model [24]. The rotor was trimmed to satisfy the given torque or thrust value in this study; however, the rotor was ideally modeled using the rigid rotor blade instead of the elastic rotor blade.

This study aims to analyze the hover performance of a coaxial co-rotating rotor using CAMRAD II with nonlinear elastic blades and the free-wake model. First, the hover performance analysis techniques for the coaxial co-rotating rotor are validated when the rotor trim approach is not applied, but the fixed collective pitch angle is used, similar to the previous references [20,21]. Second, when the rotor trim is achieved using the prescribed rotor thrust value, the hover performances, such as the rotor power (C_P/σ) and the Figure of Merit (FM), are investigated at various index angles, axial spacings, blade taper ratios, and built-in twist angles. The generic coaxial co-rotating rotor model used in references [1,20,21] is considered the baseline rotor model. In the present study, the index angle and axial spacing of the coaxial co-rotating rotor are investigated to improve the hover performance of eVTOL aircraft. The present work attempts to predict the variations in hover performances when different index angles and axial spacings are considered for the trimmed coaxial co-rotating rotor; therefore, the lower-fidelity solution by CAMRAD II with the free-wake model may be appropriate and sufficient since this analysis can provide

good calculations along with reasonable computational efficiency for rotor performances, which are the overall behaviors of a rotor.

2. Analytical Methods

2.1. Baseline Model for a Coaxial Co-Rotating Rotor

There have been no published papers on the application of actual coaxial co-rotating rotors to eVTOL aircraft. Therefore, this study uses a coaxial co-rotating rotor (Figure 4) model developed at the University of Texas at Austin (UT Austin) for the hover performance studies [1,20,21]. The general properties of the baseline rotor model are listed in Table 1, and standard atmospheric conditions are used in the present analyses.
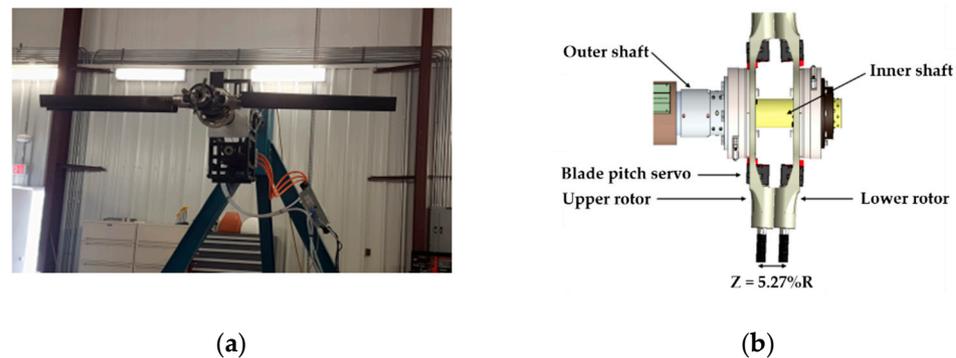

| (a) | (b) |

Figure 4. Coaxial co-rotating rotor model for test [1,20,21]: (**a**) Test stand; (**b**) rotor hub.

Table 1. Properties of the coaxial co-rotating rotor [1,20,21].

Property	Value
Hub type	Hingeless
Number of blades per rotor	2
Rotor radius, R (m)	1.108
Chord length, c (m)	0.080
Root cutout (%R)	18.76
Nominal rotor speed (RPM)	1200
Coaxial rotor solidity, σ	0.1
Airfoil	VR-12 with a tab
Taper ratio	1.0
Built-in twist angle (deg)	0.0
Pre-cone angle (deg)	3.0

2.2. Aeromechanics Modeling and Analytical Techniques

The present study uses the rotorcraft comprehensive analysis code, CAMRAD II, to model the aeromechanics and analyze the hover performance of a coaxial co-rotating rotor. The structural dynamics of the rotating blade are represented using nonlinear finite beam elements. The blade section properties can be found in the previous works [20,25]. However, the section properties at the blade root region are slightly adjusted to match the natural frequencies of the rotating blade given in a previous study [20]. Each rotor blade has 12 nonlinear finite beam elements for the analyses of structural blade dynamics. The element width near the blade root is 0.55%R, and the width near the blade tip is 2.75%R. The present coaxial co-rotating rotor does not have the swashplate, pitch link, and pitch horn, as shown in Figure 4b.

The rotor blade has a constant airfoil section using the modified VR-12 airfoil with a tab (Figure 5 [25]). The standard airfoil table for CAMRAD II modeling is generated using MSES+ [26] and XFLR [27]. In addition, Reynolds number correction [28] is used. The blade airloads are calculated using the unsteady lifting-line theory along with the wake model. In the present study, 20 aerodynamic panels are used for each rotor blade. The panel width near the blade root is 2.54%R and the width near the blade tip is 0.33%R (Figure 6).

This numerical study uses the general free-wake model to consider the aerodynamic interference effect between the upper and lower rotors. The initial vortex core radius at the blade tip in the general free-wake modeling is set as 0.5c [29]. As described previously, the unsteady lifting-line aerodynamics with the general free-wake model is a lower-order model compared to the RCAS with VVPM or CFD [20,21]. However, it is expected that CAMRAD II will reasonably and efficiently predict the hover performance of the coaxial co-rotating rotor.
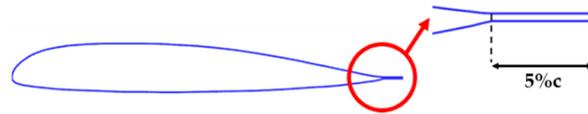

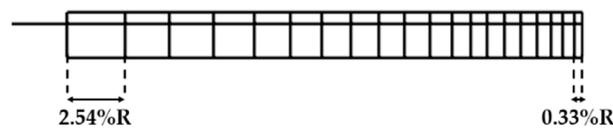**Figure 5.** Modified VR-12 airfoil with a tab [25].

Figure 6. Aerodynamic panels in CAMRAD II model.

The present numerical study considers various index angles and axial spacings (Table 2) for the hover performance analyses. A positive index angle is defined when the upper rotor is ahead of the lower rotor along the direction of rotation. Furthermore, both the upper and lower rotors rotate in the counterclockwise direction about the rotation axis from the top view. Figure 7 illustrates the CAMRAD II model of the coaxial co-rotating rotor.

Table 2. Various index angles and axial spacings.

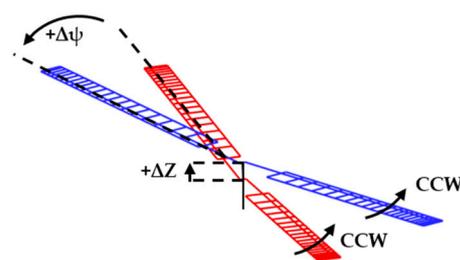| Parameter	Value
Index angle, $\Delta\Psi$ (deg)	0, ±10, ±20, ±30, ±50, ±90
Axial spacing, ΔZ (%R)	1.44, 2.17, 2.90, 5.27, 7.22, 12.60

Figure 7. CAMRAD II model for a coaxial co-rotating rotor in hover.

As noted earlier, this work studies hover performance analyses with and without the rotor trim. First, the rotor trim is not applied, but the collective pitch angle of the upper and lower rotors is fixed as 12° so that the modeling and analysis techniques are validated for the coaxial co-rotating rotor based on previous results [20,21]. Second, the rotor is trimmed to match the given thrust value of the total rotor (C_T = 0.0102) in hover. In this trim approach, the collective pitch angle of the individual rotor is used as the trim variable. For the different index angles and axial spacings of the coaxial co-rotating rotor, the hover performances, namely the rotor thrust (C_T/σ), power (C_P/σ, Equation (1)), power loading (C_T/C_P), and Figure of Merit (FM, Equation (2) [28]), are investigated. In addition, the effects of the taper ratio and built-in twist angle of the rotor blade on the hover performance

are studied for a case wherein the rotor is trimmed to satisfy the prescribed rotor thrust value. The azimuthal step of 15° is used for all calculations in this study.

$$P = P_i + P_{\text{int}} + P_o \tag{1}$$

$$FM = \frac{(C_{T,upper} + C_{T,lower})^{3/2}}{\sqrt{2}(C_{P,upper} + C_{P,lower})} \tag{2}$$

3. Results

3.1. Fan Plot Analyses

Prior to the performance analyses in hover using CAMRAD II, the natural frequencies of a rotating blade of the coaxial co-rotating rotor are predicted and compared to the previous predictions [20] to validate the structural dynamics of the rotor system, as shown in Figure 8a. Based on this figure, the predictions using CAMRAD II are consistent with the blade's natural frequencies obtained using RCAS [20]. Additionally, Figure 8b shows the mode shapes of a rotor blade at the nonrotating condition. Therefore, it is believed that the present modeling of the structural dynamics for the coaxial co-rotating rotor is reasonable.
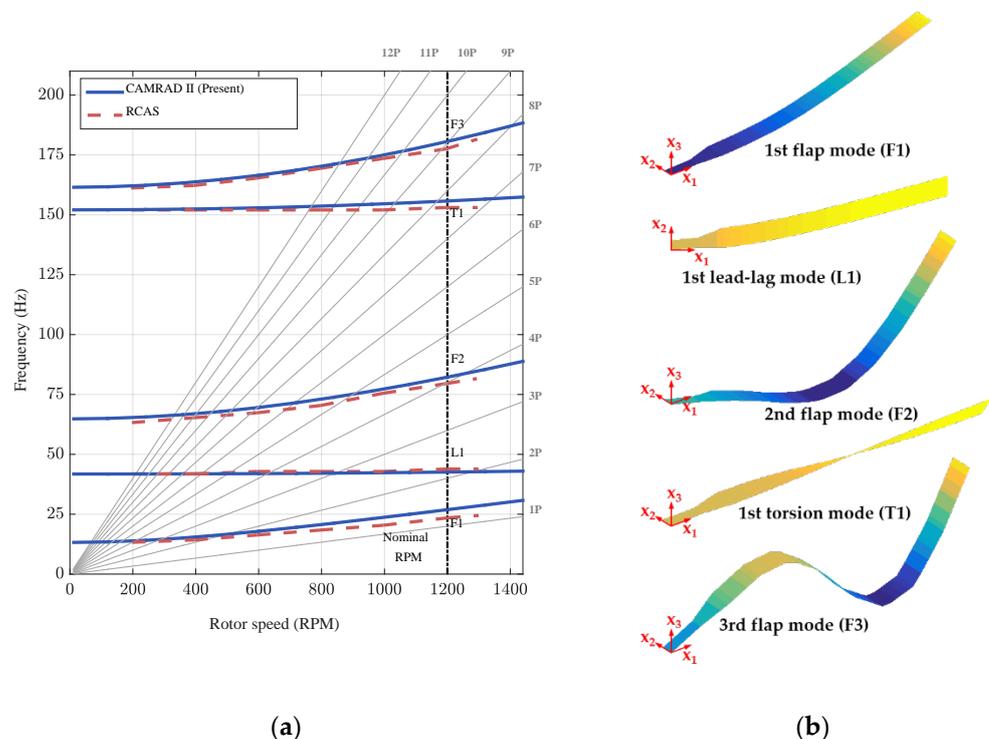

Figure 8. Validation for natural frequencies of rotating blade with RCAS [20]: (**a**) Fan plot; (**b**) mode shapes at the nonrotating condition.

3.2. Hover Performance Analyses without Trim Techniques

In this section, hover performance analyses using CAMRAD II are first validated against previously obtained results [21] for the case when the rotor trim is not applied, but the collective pitch angle of 12° is fixed. Figure 9 shows the variations in the rotor thrust and power loading in terms of the index angle at a fixed axial spacing of 5.27%R, which is a relatively small axial spacing. As shown in Figure 9a,b, the thrust variations of the lower and upper rotors are symmetric relative to each other with an increase in the index angle, which is consistent with the result of previous work [21]. Furthermore, the individual rotor thrust changes sharply in the index angle region of −10° to 10°. Figure 9c,d indicates that the trends for both the total rotor thrust and power loading in terms of the index angle are similar to previous results, obtained experimentally and by using RCAS with

VVPM [21]. As depicted in Figure 9, the relationship between the hover performance and the index angle is comparable to that observed in the previous work, but the rotor thrust magnitude and power loading magnitude are different from the test results, as shown in the previous study [21]. The magnitudes of the results obtained using RCAS with VVPM and the experiment [21] differ by approximately 10%. These differences may be due to the following reasons. Firstly, imperfections in the blade pitch grip or actuators at the test could result in these differences. Secondly, the rotor power could not be predicted accurately owing to the turbulence model used in the RCAS with VVPM. In the present predictions, the unsteady lifting-line theory along with the free-wake model in CAMRAD II is a lower-order model compared with the RCAS with VVPM; thus, as reported in the previous work [21], the present analysis shows a difference in the measured results. In addition, there is a difference in the increment of the index angle ($\Delta\Psi$) used for the present prediction, the previous test, and the RCAS analysis [21], which may result in the difference of the index angle value for the maximum rotor thrust value. However, the present trends in terms of the index angle by CAMRAD II are similar to the results of the previous study [21]. Therefore, it can be considered that the CAMRAD II analysis with the free-wake model can appropriately predict the hover performance of a coaxial co-rotating rotor. In addition, the validation of the hover performance in the previous work [21] shows that the CAMRAD II modeling is appropriate.
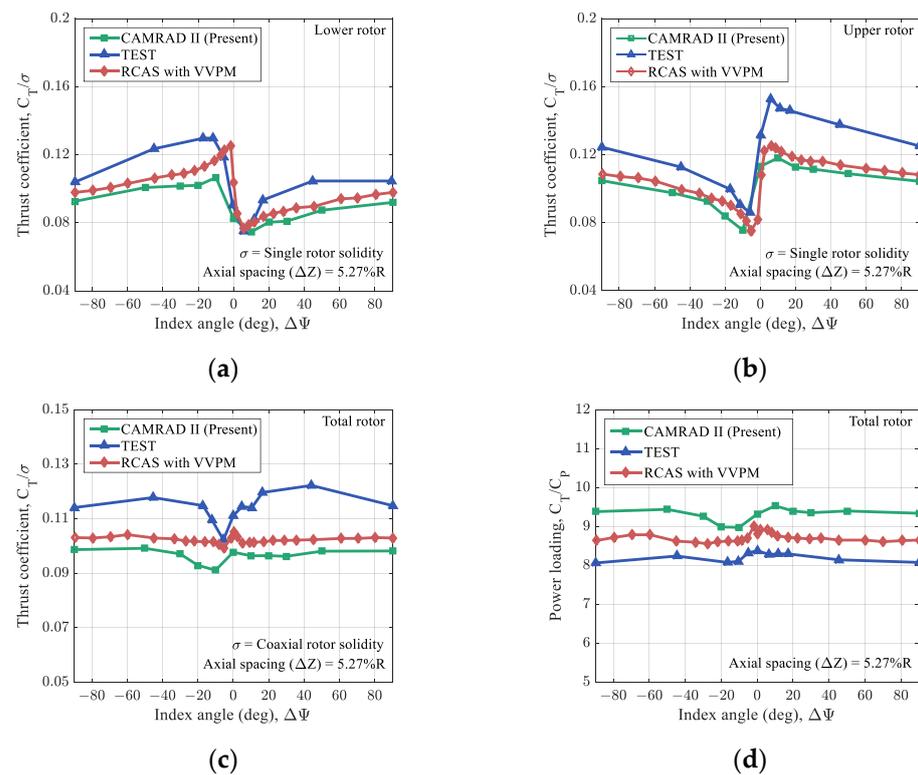

Figure 9. Validation for hover performance analyses of coaxial co-rotating rotor in terms of index angle with previous results [21] (collective pitch angle = 12°): (**a**) Lower rotor thrust (C_T/σ); (**b**) upper rotor thrust (C_T/σ); (**c**) total rotor thrust (C_T/σ); (**d**) total rotor power loading (C_T/C_P).

Second, using the CAMRAD II model, which is validated in the previous example, hover performance analyses are conducted without the rotor trim, considering wider ranges of the index angle and axial spacing. Figure 10 shows the results for the total rotor thrust, power, and power loading when various index angles and axial spacings are considered. For an axial spacing of less than 5.27%R, which is a relatively smaller axial spacing, the maximum rotor thrust is generated close to an index angle of 0° (Figure 10a). However, when the axial spacing exceeds 5.27%R, which is a relatively larger axial spacing,

the maximum rotor thrust is observed close to an index angle of $50°$, as illustrated in Figure 10a. For the rotor power (Figure 10b), when the axial spacing is less than $5.27\%R$, the minimum value is obtained near an index angle of $-10°$. In addition, the minimum rotor power is found close to an index angle of $10°$ when the axial spacing is greater than $5.27\%R$. Figure 10c indicates the total rotor power loading for various index angles and axial spacings. Similar to the total rotor thrust variation, shown in Figure 10a, the maximum rotor power loading is produced close to the index angles of $0°$ and $50°$ when the axial spacing is lower than $5.27\%R$ and higher than $5.27\%R$, respectively. Therefore, the hover performance of the coaxial co-rotating rotor can be changed by adjusting the index angle or the axial spacing.
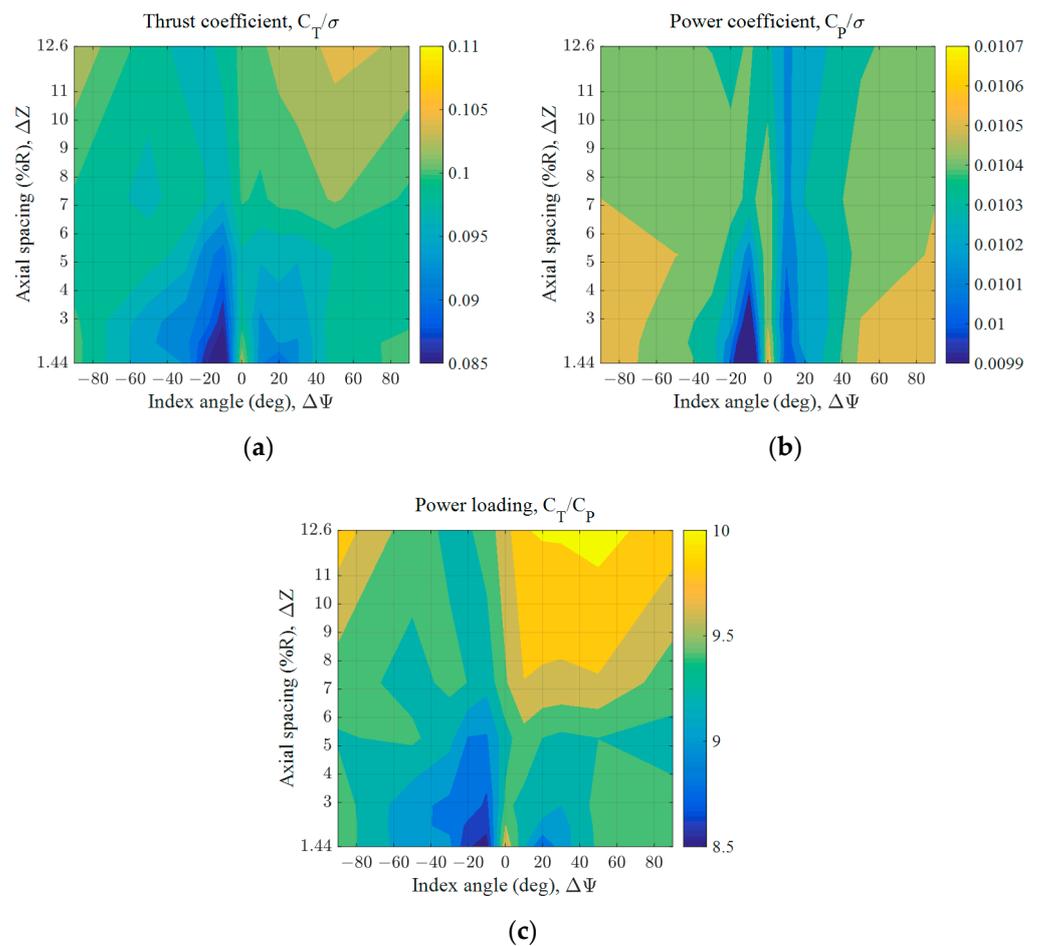

(a)

(b)

(c)

Figure 10. Hover performance analyses with respect to various index angles and axial spacings (collective pitch angle = $12°$): (**a**) Thrust (C_T/σ); (**b**) power (C_P/σ); (**c**) power loading (C_T/C_P).

Figure 11 shows the contributions of the rotor power components to the total rotor power (Figure 10b) when different index angles and axial spacings are considered. As defined in Equation (1), the rotor power (C_P/σ) is composed of the induced power (C_{Pi}/σ), interference power (C_{Pint}/σ), and profile power (C_{Po}/σ). Similar to the results presented in Figure 10b, when the axial spacing is lower than $5.27\%R$, the minimum induced power and interference power are both obtained close to an index angle of $-10°$. In addition, when the axial spacing is higher than $5.27\%R$, the minimum induced power and interference power are observed close to an index angle of $10°$ (Figure 11a,b). The profile power magnitude (Figure 11c) is relatively lower than the induced power and interference power. Thus, its contribution to the total power is not significant compared with other power components. When comparing Figure 10b with Figure 11a,b, the variations in the induced power and interference power are similar to that of the total power. However, the interference power

magnitude is lower than the induced power magnitude. Therefore, it is shown that the induced power exerts the highest influence on the total power, and the interference power exerts the second most important influence on the total power.
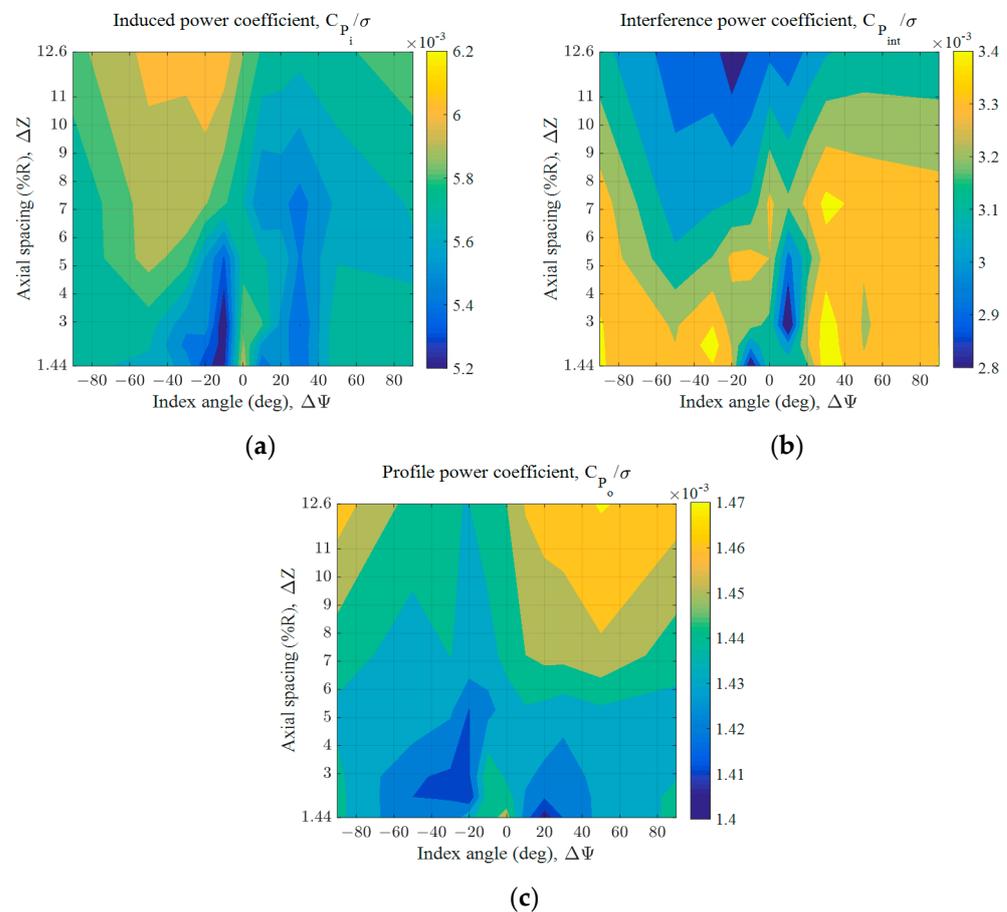

Figure 11. Rotor power components with different index angles and axial spacings (collective pitch angle = 12°): (**a**) Induced power (C_{Pi}/σ); (**b**) interference power (C_{Pint}/σ); (**c**) profile power (C_{Po}/σ).

3.3. Hover Performance Analyses with Trim Techniques

3.3.1. Hover Performance Analyses

In this section, hover performance analyses for a coaxial co-rotating rotor using CAM-RAD II when the rotor is trimmed to match the given thrust value of the total rotor (C_T = 0.0102) are described. This thrust value is based on the measured thrust value in previous studies [20,21]. As previously stated, the individual rotor's collective pitch angle is used as the trim variable. Figure 12 shows the variations in the rotor thrust and power in terms of the index angle at a fixed axial spacing of 5.27%R, which is a relatively small axial spacing. As given in Figure 12a, the thrust variations of the lower and upper rotors are symmetric relative to each other with respect to the horizontal axis; this can be observed in the hover performance analyses results without the trim (Figure 9a,b). In addition, the maximum lower rotor thrust and the upper rotor thrust are obtained at an index angle of −10° and 10°, respectively. The minimum total rotor power is found at an index angle of 10°, as shown in Figure 12b. When the axial spacing is 5.27%R, the minimum total rotor power without the trim is also generated at an index angle of 10° (Figure 10b). Furthermore, the total rotor power decreases by 6.50% as the index angle increases from −10° to 10° (Figure 12b).
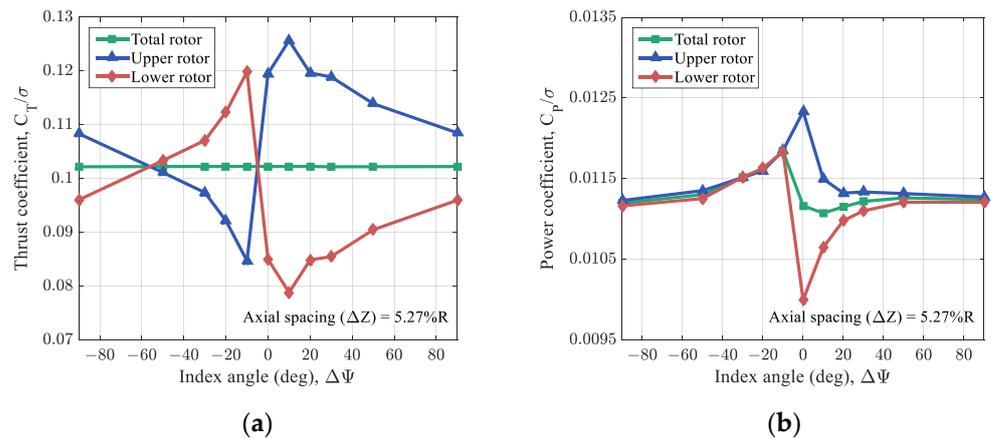
Figure 12. Hover performance analyses in terms of index angle (C_T = 0.0102): (**a**) Thrust (C_T/σ); (**b**) power (C_P/σ).

Figures 13 and 14 present the hover performance results for the coaxial co-rotating rotor trimmed for the prescribed rotor thrust value (C_T = 0.0102) when various index angles and axial spacings are considered. Figure 13 shows the hover performance results including the total rotor power and FM for the various index angles and axial spacings. For an axial spacing of less than 5.27%R, which is a relatively small value, the minimum rotor power is obtained near an index angle of 0° (Figure 13a). On the contrary, when the axial spacing exceeds 5.27%R, which is a relatively large axial spacing, the minimum rotor power is produced near an index angle of 10°, as shown in Figure 13a. The overall predicted rotor power magnitude when the trim technique is applied (Figure 13a) is relatively higher than the result observed when the trim method is not applied, as shown in Figure 10b. Figure 13b shows the FM of the total rotor (Equation (2)) with respect to the various index angles and axial spacings. The maximum value of FM is found near an index angle of 0° and 10° when the axial spacing is lower than 5.27%R and higher than 5.27%R, respectively. Therefore, it is concluded that the hover performance of the coaxial co-rotating rotor can be changed by adjusting the index angle or the axial spacing, even when the rotor trim technique is applied, similar to Figure 10 presented in Section 3.2 without the rotor trim.
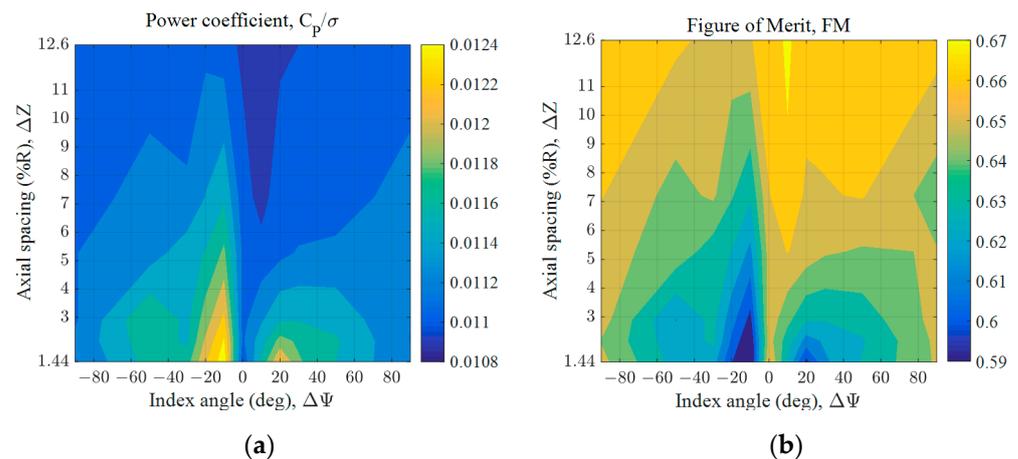

Figure 13. Hover performance analyses with respect to various index angles and axial spacings (C_T = 0.0102): (**a**) Power (C_P/σ); (**b**) Figure of Merit (FM).

Figure 14 shows the contributions of the rotor power components to the total rotor power (Figure 13a) when various index angles and axial spacings are considered to be similar to those in Figure 11 without the rotor trim. Similar to the rotor power in Figure 13a, when the axial spacing is less than 5.27%R, both the minimum induced power and interference power are obtained near an index angle of 0°. In addition, when the axial spacing

exceeds 5.27%R, they are observed close to an index angle of 10° (Figure 14a,b). However, similar to Figure 11 in Section 3.2, the profile power magnitude (Figure 14c) is relatively lower than that of the other power components. Therefore, its effect on the total rotor power is insignificant compared with the induced and interference powers. In addition, similar to Figure 11, the trends in the induced power and interference power are comparable with the variation in the total power depicted in Figure 13a. However, the magnitude of induced power is higher than that of the interference power. Thus, it is observed that the effect of the induced power on the total power is the most dominant, and the effect of the interference power on the total power follows next. For the results obtained without and with the rotor trim method (Figures 11 and 14), the rotor power components change with the index angle or the axial spacing. However, as shown in Figure 14, the magnitude of the rotor power components with the rotor trim is higher than the results without the rotor trim, shown in Figure 11.
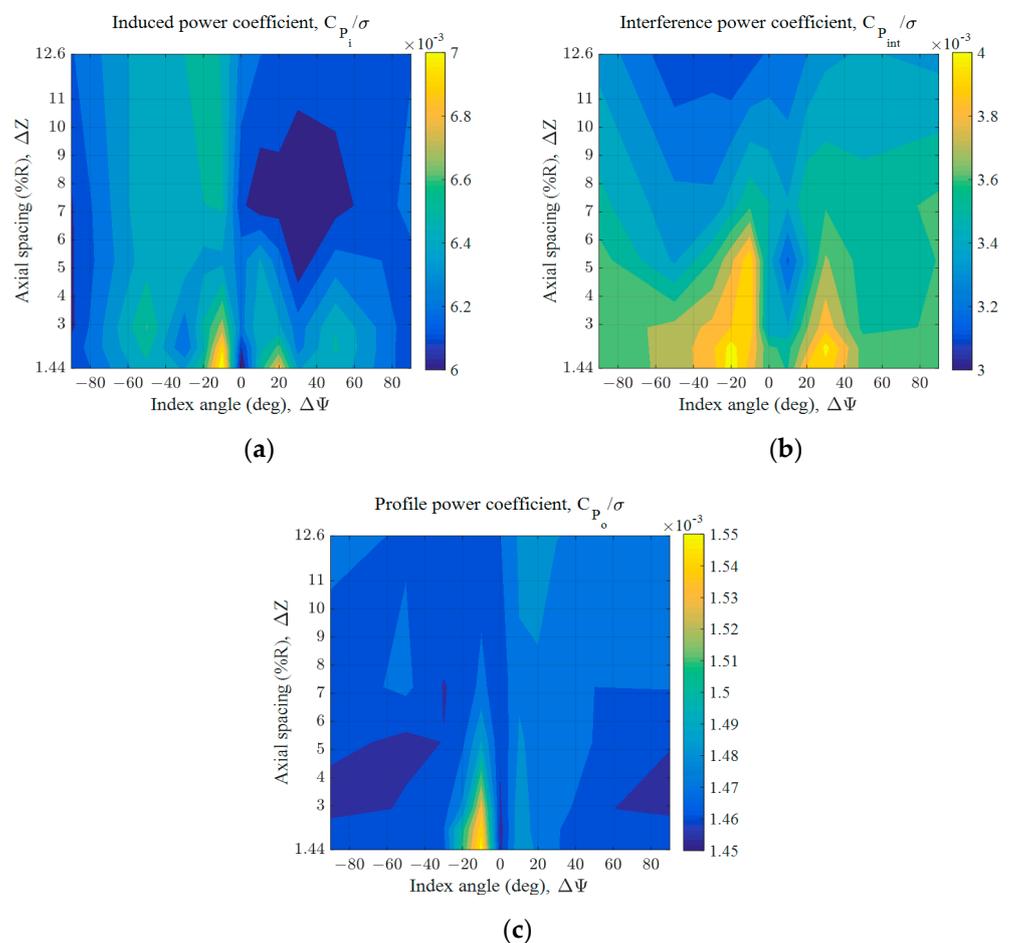

(a)

(b)

(c)

Figure 14. Rotor power components with different index angles and axial spacings (C_T = 0.0102): (**a**) Induced power (C_{Pi}/σ); (**b**) interference power (C_{Pint}/σ); (**c**) profile power (C_{Po}/σ).

3.3.2. Blade Load Analyses

In this section, blade load analyses, such as the blade structural loads and airloads, are explained for when the previously described rotor trim approach is applied. In this load analysis, the index angles of $-10°$ and $10°$ are considered because the maximum thrusts of the lower and upper rotors are obtained at these values, respectively, at a fixed axial spacing of 5.27%R (Figure 12a). The blade flap bending moment (M_Y) is investigated considering the hover condition, and the positive flap bending moment is defined when the blade is bent upwards in this study. Figure 15 shows the flap bending moment for each rotor with index angles of $-10°$ and $10°$ at an axial spacing of 5.27%R. As given in Figure 15a, the

flap bending moment in the inboard region of the lower rotor is higher than that of the upper rotor because the lower rotor thrust is higher than the upper rotor thrust at an index angle of $-10°$ (Figure 12a). In contrast, as seen in Figure 15b, the flap bending moment in the inboard region for the lower rotor is lower than that of the upper rotor because the lower rotor thrust is lower than the upper rotor thrust at an index angle of $10°$, as shown in Figure 12a. Therefore, it is considered that the blade's structural loads can be controlled by adjusting the index angle, similar to the rotor hover performance depicted in Figures 12–14.
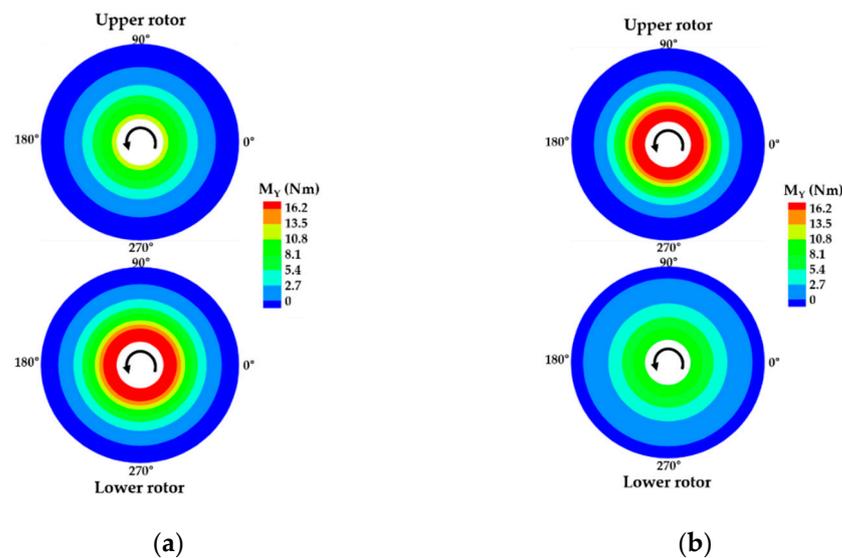

Figure 15. Flap bending moment (M_Y) distributions at the axial spacing of 5.27%R (C_T = 0.0102): (**a**) Index angle = $-10°$; (**b**) index angle = $10°$.

Figure 16 shows the non-dimensional section lift force (M^2C_l) of the upper and lower rotors with index angles of $-10°$ and $10°$ at an axial spacing of 5.27%R. As previously presented in Figure 12a, the lower rotor thrust is higher than the upper rotor thrust at an index angle of $-10°$, and the upper rotor thrust is higher than that of the lower rotor at an index angle of $10°$. Therefore, the section lift force in the blade outboard region for the lower rotor is higher than that of the upper rotor at an index angle of $-10°$ in Figure 16a. Moreover, the section lift force in the outboard region for the lower rotor is lower than M^2C_l for the upper rotor at an index angle of $10°$ (Figure 16b). Thus, the blade's airloads can also be changed by adjusting the index angle, similar to the structural loads (Figure 15).

3.3.3. Effect of the Taper Ratio on Hover Performance

It is well known that the rotor efficiency in hover can increase when a taper is applied to the rotor blade [30]. Therefore, the effect of the taper ratio is studied on the hover performance of a coaxial co-rotating rotor trimmed to match C_T = 0.0102. A taper ratio of 0.8 is considered, and the results with and without the blade taper are compared to each other. Figure 17 shows the hover performance analyses for a taper ratio of 0.8. As shown in the figure, the trends for the total rotor power and the FM with respect to the various index angles and axial spacings are similar to the results obtained without the blade taper in Figure 13. However, the rotor power magnitude and FM magnitude are different from those in Figure 13. As shown in Figure 17a, the rotor power decreases by 3.17% as the taper ratio decreases from 1.0 (Figure 13a) to 0.8 at an index angle of $0°$ and axial spacing of 1.44%R. In addition, the power decreases by 2.37% at an index angle of $10°$ and axial spacing of 12.6%R. However, the FM increases by 3.03% as the taper ratio decreases from 1.0 (Figure 13b) to 0.8 at an index angle of $0°$ and axial spacing of 1.44%R (Figure 17b). Furthermore, as given in Figure 17b, the FM increases by 2.99% at an index angle of $10°$

and axial spacing of 12.6%R. Therefore, it is considered that the hover performance of the coaxial co-rotating rotor can be improved when a taper is applied to the blade.
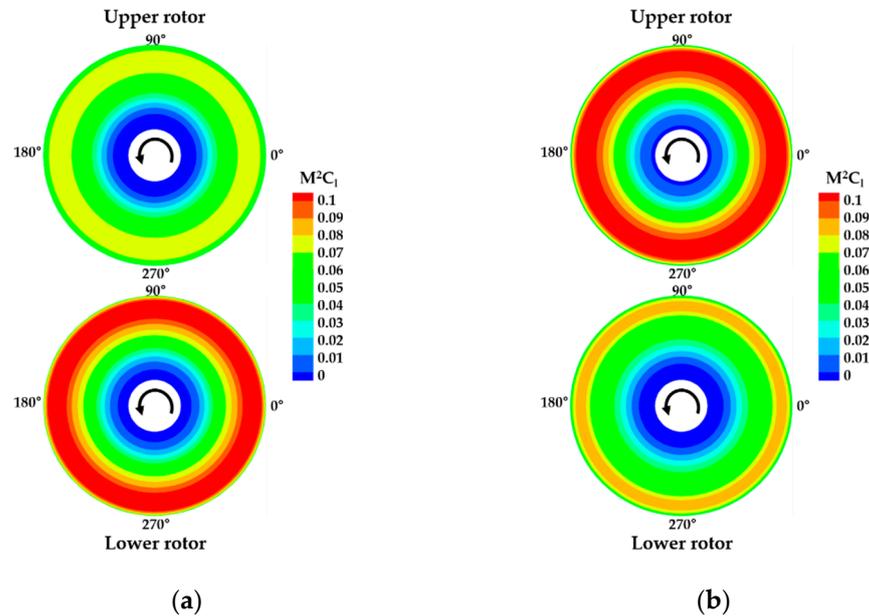

Figure 16. Section lift force (M^2C_l) distributions at the axial spacing of 5.27%R ($C_T = 0.0102$): (**a**) Index angle = $-10°$; (**b**) index angle = $10°$.
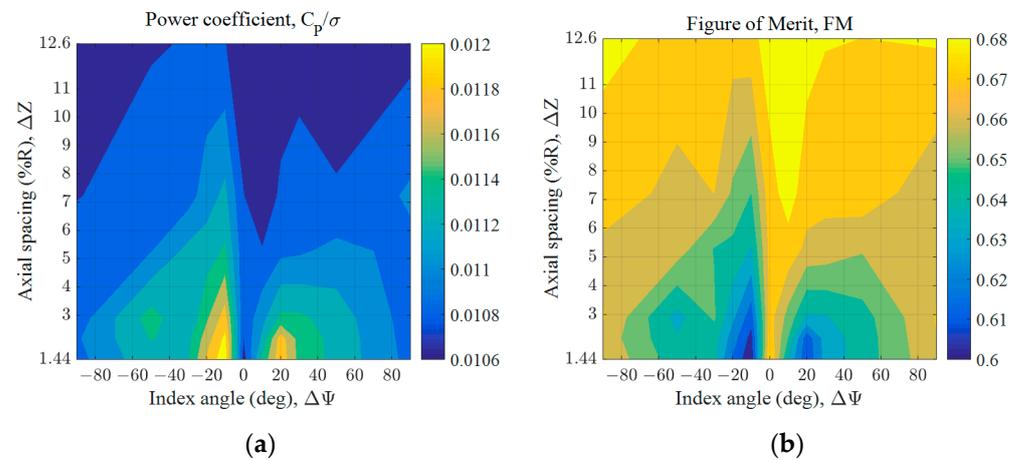

Figure 17. Hover performance analyses with respect to various index angles and axial spacings with blade taper ratio = 0.8 ($C_T = 0.0102$): (**a**) Power (C_P/σ); (**b**) Figure of Merit (FM).

3.3.4. Effect of the Built-In Twist on Hover Performance

When the built-in twist (or pre-twist) for the blade is appropriately applied, the rotor hover performance can be improved [30]. Therefore, the effect of the built-in twist angle on the hover performance for the coaxial co-rotating rotor trimmed with a given rotor thrust ($C_T = 0.0102$) is investigated. The linear built-in twist angle is assumed to be $-12°$ for comparison with the results without the built-in twist. Figure 18 shows the hover performance results using a built-in twist angle of $-12°$. As observed in the figure, the trends for the total rotor power and the FM with respect to the various index angles and axial spacings are similar to those obtained without the built-in twist (Figure 13). However, similar to Section 3.3.3, the magnitudes of the rotor power and FM are different from the results presented in Figure 13. As shown in Figure 18a, the power decreases by 5.91% when a built-in twist angle of $-12°$ is considered at an index angle of $0°$ and axial spacing of 1.44%R. In addition, the power decreases by 5.84% at an index angle of $10°$ and axial

spacing of 12.6%R. On the contrary, the FM increases by 6.06% at an index angle of 0° and axial spacing of 1.44%R when the built-in twist angle is −12° (Figure 18b). Furthermore, the FM increases by 5.97% at an index angle of 10° and axial spacing of 12.6%R, as shown in Figure 18b. The hover performance of the coaxial co-rotating rotor can be improved when a built-in twist angle is applied. Moreover, compared to Section 3.3.3 in which a blade taper ratio of 0.8 is used, the FM for a built-in twist angle of −12° is 2.94% higher at an index angle of 0° and axial spacing of 1.44%R. In addition, the FM with the built-in twist is improved by 2.90% compared with the case in which a blade taper ratio is used at an index angle of 10° and axial spacing of 12.6%R. Therefore, when the built-in twist angle is used, the hover performance is significantly improved compared with the tapered blade. The trend in the hover performance in terms of the index angle or the axial spacing is maintained, although the blade planform is modified.
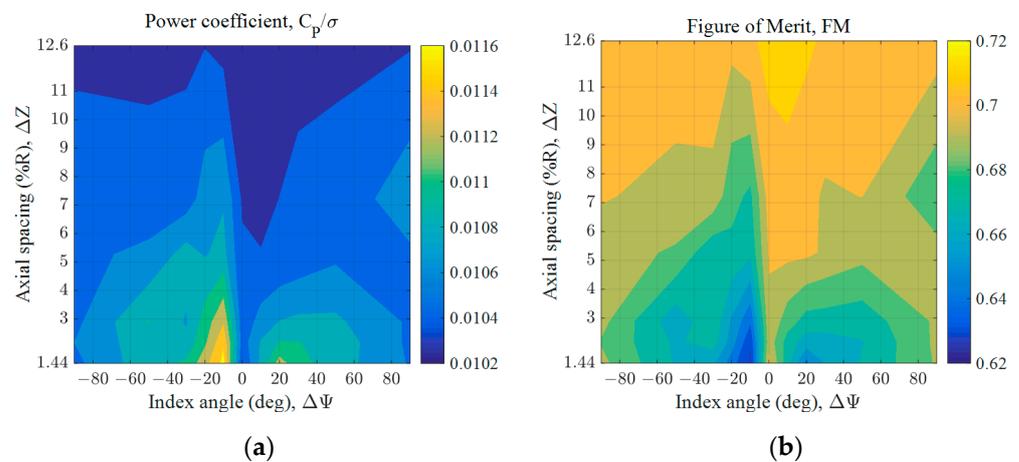

Figure 18. Hover performance analyses with respect to various index angles and axial spacings with built-in twist angle = −12° (C_T = 0.0102): (**a**) Power (C_P/σ); (**b**) Figure of Merit (FM).

4. Conclusions

In the present study, hover performance analyses of coaxial co-rotating rotors for application to eVTOL aircraft were conducted using CAMRAD II with the free-wake model. A generic coaxial co-rotating rotor without the blade taper and the built-in twist was used as the baseline model. This study considered the hover performance with and without the rotor trim technique.

First, when the rotor trim was not applied, but a constant collective pitch angle of 12° was used for the upper and lower rotors, the hover performances, including the rotor thrust and power loading, were successfully validated against previously studied test data and analyses. Using the validated CAMRAD II model, hover performance analyses were conducted considering wide ranges of the index angle and axial spacing. The maximum rotor power loading was observed close to an index angle of 0° when the axial spacing was less than 5.27%R. In addition, as the axial spacing exceeded 5.27%R, the maximum power loading was obtained near an index angle of 50°. Thus, this numerical study demonstrated that the hover performance of a coaxial co-rotating rotor could be changed by adjusting the index angles or the axial spacings when the rotor was not trimmed.

Second, for the rotor trimmed to match the prescribed rotor thrust value (C_T = 0.0102), the hover performances were investigated considering different index angles, axial spacings, blade taper ratios, and built-in twist angles. When the axial spacing was lower and higher than 5.27%R, the rotor FM was maximized near an index angle of 0° and 10°, respectively. It was shown that the hover performance could be changed by adjusting the index angles or the axial spacings when the rotor was trimmed, similar to the results obtained without the rotor trim. Compared with the results obtained without the blade taper, the maximum value of the FM with a taper ratio of 0.8 increased by 3.03% when the index angle was 0°,

and the axial spacing was 1.44%R. In addition, the maximum FM with a blade built-in twist angle of $-12°$ increased by 6.06% when the index angle was $0°$, and the axial spacing was 1.44%R. Furthermore, it was studied that the blade flap bending moments and sectional lift forces were different or changed for the index angles.

Although a relatively lower-order model, the free-wake model, was used in the present work compared with the previous studies using the RCAS with VVPM or CFD, the validation for hover performance of the coaxial co-rotating rotor was reasonable. Furthermore, the hover performances were investigated when the rotor trim was applied to satisfy the given rotor thrust value, considering different index angles, axial spacings, blade taper ratios, and built-in twist angles. In the future, the rotor inflow distribution and vortex trajectory from rotating blades when the coaxial co-rotating rotor is trimmed will be studied such that the reason for changes in the hover performance is investigated.

Author Contributions: Conceptualization, J.-S.P.; methodology, J.-S.P.; software, Y.-B.L.; validation, Y.-B.L.; formal analysis, Y.-B.L.; investigation, Y.-B.L.; resources, J.-S.P.; data curation, Y.-B.L.; writing—original draft preparation, Y.-B.L.; writing—review and editing, J.-S.P.; visualization, Y.-B.L.; supervision, J.-S.P.; funding acquisition, J.-S.P. All authors have read and agreed to the published version of the manuscript.

Institutional Review Board Statement: Not applicable.

Informed Consent Statement: Not applicable.

Data Availability Statement: The numerical data used to support the findings of this study are included in the article.

Conflicts of Interest: The authors declare no conflict of interest.

Nomenclature

R	Rotor radius, m
c	Blade chord length, m
σ	Coaxial rotor solidity
$\Delta\Psi$	Index angle, deg
ΔZ	Axial spacing, %R
M_Y	Flap bending moment, Nm
M	Local Mach number
C_l	Sectional lift force coefficient
C_T	Rotor thrust coefficient
C_P	Rotor power coefficient
C_{P_i}	Rotor induced power coefficient
$C_{P_{int}}$	Rotor interference power coefficient
C_{P_o}	Rotor profile power coefficient
C_T/C_P	Rotor power loading
FM	Rotor Figure of Merit

References

1. Johnson, C.; Sirohi, J.; Jacobellis, G.; Singh, R.; McDonald, R. Investigation of stacked rotor performance in hover part 1: Experimental measurements. In Proceedings of the VFS Aeromechanics for Advanced Vertical Flight Technical Meeting, San Jose, CA, USA, 21–23 January 2020.
2. The Electric VTOL NewsTM. Available online: https://evtol.news/ (accessed on 7 December 2021).
3. Bain, J.; Mikić, G.V.; Stoll, A. Aerodynamic and acoustic design of the Joby aviation eVTOL propeller. In Proceedings of the Vertical Flight Society's 77th Annual Forum and Technology Display, Virtual, 10–14 May 2021.
4. Holden, J.; Goel, N. Fast-forwarding to a future of on-demand urban air transportation. In Proceedings of the UBER Elevate, San Francisco, CA, USA, 27 October 2016.

5. Sorensen, P.; Cuppoletti, D.R. Rotor-rotor interaction noise of counter-rotating vs. co-rotating rotors for air mobility applications. In Proceedings of the AIAA SCITECH 2022 Forum, San Diego, CA, USA, 3–7 January 2022.

6. Antcliff, K.; Whiteside, S.; Kohlman, L.W.; Silva, C. Baseline assumptions and future research areas for urban air mobility vehicles. In Proceedings of the AIAA SCITECH 2019 Forum, San Diego, CA, USA, 7–11 January 2019.

7. Pollard, B.; Patterson, M.D.; Whiteside, S. A combined blade element and vortex panel method for stacked rotor analysis. In Proceedings of the AIAA AVIATION Forum, Dallas, TX, USA, 17–21 June 2019.

8. Tinney, C.E.; Valdez, J. Thrust and Acoustic Performance of Small-Scale, Coaxial, Corotating Rotors in Hover. *AIAA J.* **2020**, *58*, 1657–1667. [CrossRef]

9. Platzer, S.; Hajek, M.; Rauleder, J.; Mortimer, P.; Sirohi, J. Investigation of the flow fields of coaxial stacked and counter-rotating rotors using PIV measurements and URANS simulations. In Proceedings of the Vertical Flight Society's 77th Annual Forum and Technology Display, Virtual, 10–14 May 2021.

10. Valdez, J.A.; Tinney, C.E. The unsteady wake produced by a coaxial co-rotating rotor in hover. In Proceedings of the AIAA SCITECH 2022 Forum, San Diego, CA, USA, 3–7 January 2022.

11. Kunz, D.L.; Newkirk, M.C. A Generalized Dynamic Balancing Procedure for the AH-64 Tail Rotor. *J. Sound Vib.* **2009**, *326*, 353–366. [CrossRef]

12. Jacobellis, G.; Singh, R.; Johnson, C.; Sirohi, J. Experimental and computational investigation of stacked rotor broadband noise in hover. In Proceedings of the VFS 77th Annual Forum, Virtual, 10–14 May 2021.

13. Misiorowski, M.; Gandhi, F.; Anusonti-Inthra, P. Comparison of acoustic predictions using distributed and compact airloads. In Proceedings of the Vertical Flight Society 75th Annual Forum and Technology Display, Philadelphia, PA, USA, 13–16 May 2019.

14. Bhagwat, M. Co-rotating and counter-rotating coaxial rotor performance. In Proceedings of the AHS Specialists' Conference on Aeromechanics Design for Transformative Vertical Flight, San Francisco, CA, USA, 16–18 January 2018.

15. Whiteside, S.K.S.; Zawodny, N.S.; Fei, X.; Pettingill, N.A.; Patterson, M.D.; Rothhaar, P.M. An exploration of the performance and acoustic characteristics of UAV-scale stacked rotor configurations. In Proceedings of the AIAA SCITECH 2019 Forum, San Diego, CA, USA, 7–11 January 2019.

16. Uehara, D.; Sirohi, J.; Bhagwat, M.J. Hover Performance of Corotating and Counterrotating Coaxial Rotors. *J. Am. Helicopter Soc.* **2020**, *65*, 1–8. [CrossRef]

17. Uehara, D.; Sirohi, J. Quantification of swirl recovery in a coaxial rotor system. In Proceedings of the AHS International 73rd Annual Forum & Technology Display, Fort Worth, TX, USA, 9–11 May 2017.

18. Ramasamy, M. Hover Performance Measurements toward Understanding Aerodynamic Interference in Coaxial, Tandem, and Tilt Rotors. *J. Am. Helicopter Soc.* **2015**, *60*, 1–17. [CrossRef]

19. Brazinskas, M.; Prior, S.D.; Scanlan, J.P. An Empirical Study of Overlapping Rotor Interference for a Small Unmanned Aircraft Propulsion System. *Aerospace* **2016**, *3*, 32. [CrossRef]

20. Jacobellis, G.; Singh, R.; Johnson, C.; Sirohi, J.; McDonald, R. Experimental and Computational Investigation of Stacked Rotor Performance in Hover. *Aerosp. Sci. Technol.* **2021**, *116*, 106847. [CrossRef]

21. Jacobellis, G.; Singh, R.; Johnson, C.; Sirohi, J.; McDonald, R. Investigation of stacked rotor performance in hover pt. II: Computational validation. In Proceedings of the AHS Aeromechanics Specialists' Meeting, San Jose, CA, USA, 21–23 January 2020.

22. Saberi, H.; Khoshlahjeh, M.; Ormiston, R.A.; Rutkowski, M.J. Overview of RCAS and application to advanced rotorcraft problems. In Proceedings of the AHS 4th Decennial Specialist's Conference on Aeromechanics, San Francisco, CA, USA, 21–23 January 2004.

23. Johnson, W. *CAMRAD II, Comprehensive Analytical Model of Rotorcraft Aerodynamics and Dynamics*; Johnson Aeronautics: Palo Alto, CA, USA, 1992.

24. Lee, Y.-B.; Park, J.-S. Study on Performance Analyses on Coaxial Co-Rotating Rotors of e-VTOL Aircraft for Urban Air Mobility. *J. Korean Soc. Aeronaut. Space Sci.* **2021**, *49*, 1011–1018. [CrossRef]

25. Schmaus, J.H. Aeromechanics of a High Speed Coaxial Helicopter Rotor. Ph.D. Thesis, University of Maryland, College Park, MD, USA, 2017.

26. Drela, M. *A User's Guide to MSES 3.05*; MIT Department of Aeronautics and Astronautics: Cambridge, MA, USA, 2007.

27. XFLR5. *Analysis of Foils and Wings Operating at Low Reynolds Numbers*; XFLR5 v6.02 Guidelines; MIT Aerospace Computational Design Laboratory: Cambrige, MA, USA, 2013.

28. Lim, J.W.; McAlister, K.W.; Johnson, W. Hover Performance Correlation for Full-Scale and Model-Scale Coaxial Rotors. *J. Am. Helicopter Soc.* **2009**, *54*, 32005. [CrossRef]

29. Go, J.-I.; Kim, D.-H.; Park, J.-S. Performance and Vibration Analyses of Lift-Offset Helicopters. *Int. J. Aerosp. Eng.* **2017**, *2017*, 1865751. [CrossRef]

30. Leishman, G.J. *Principles of Helicopter Aerodynamics*; Cambridge University Press: Cambridge, UK, 2006.